

Blind Identification of SFBC-OFDM Signals Using Subspace Decompositions and Random Matrix Theory

Mingjun Gao, *Student Member, IEEE*, Yongzhao Li, *Senior Member, IEEE*,
Octavia A. Dobre, *Senior Member, IEEE*, and Naofal Al-Dhahir, *Fellow, IEEE*

Abstract—Blind signal identification has important applications in both civilian and military communications. Previous investigations on blind identification of space-frequency block codes (SFBCs) only considered identifying Alamouti and spatial multiplexing transmission schemes. In this paper, we propose a novel algorithm to identify SFBCs by analyzing discriminating features for different SFBCs, calculated by separating the signal subspace and noise subspace of the received signals at different adjacent OFDM sub-carriers. Relying on random matrix theory, this algorithm utilizes a serial hypothesis test to determine the decision boundary according to the maximum eigenvalue in the noise subspace. Then, a decision tree of a special distance metric is employed for decision making. The proposed algorithm does not require prior knowledge of the signal parameters such as the number of transmit antennas, channel coefficients, modulation mode and noise power. Simulation results verify the viability of the proposed algorithm for a reduced observation period with an acceptable computational complexity.

Index Terms—Blind identification, space-frequency block codes, orthogonal frequency division multiplexing.

I. INTRODUCTION

DUE to its increasing civilian and military applications, blind identification of communication signal parameters without reference signals has received increased attention recently. Military applications include blind identification of potentially hostile communication sources in radio surveillance, interference identification, electronic warfare and forensics for securing wireless communications [1], [2]. In the context of civilian use, employing blind identification algorithms at the receiver is critical for software defined radios and cognitive radios to improve power and spectral efficiencies [1]. Recently, numerous algorithms have been developed for the blind identification of multiple-input-multiple-output (MIMO) signal parameters such as the number of transmit antennas [3]–[5] and space-time block codes (STBC) [6]–[21].

Previously reported investigations on the identification of STBC include references [6]–[15] for single-carrier systems and references [16]–[21] for orthogonal frequency division multiplexing (OFDM) systems. Regarding the identification of STBC for single-carrier systems, previous works can be divided into two types of algorithms: likelihood-based [6] and feature-based [7]–[15] algorithms. All of these algorithms are not applicable to OFDM systems over frequency selective fading channels as shown in Fig. 1.a. As for OFDM systems, there are two major spatial transmit diversity approaches. The first is STBC-OFDM which implements the spatial redundancy

over adjacent OFDM symbols and has been adopted in indoor WiFi standards [22], [23]. However, under high mobility scenarios, implementing the STBC over adjacent OFDM symbols is ineffective due to the significant channel time variations. Instead, another spatial transmit diversity approach, namely, space-frequency block code (SFBC), is considered where the spatial redundancy is implemented over adjacent OFDM sub-carriers within the same OFDM symbol. Several wireless standards, such as LTE [24] and WiMAX [25], [26], have adopted SFBC-OFDM. In [16]–[18], the authors proposed detecting the peak of the cross-correlation function in the time-domain to identify STBC-OFDM signals. However, the time-domain cross-correlation between adjacent OFDM symbols does not exist any longer for SFBC-OFDM signals. Thus, blind identification algorithms of STBC-OFDM cannot be directly applied to SFBC-OFDM signals as shown in Fig. 1.b. The authors of [19], [21] apply the principle of STBC-OFDM identification to the SFBC scenario. These algorithms detect the peak of the cross-correlation in one OFDM symbol. However, they can only identify a small number of SFBCs due to the identical location of the peak for many SFBCs. To tackle this challenge, our prior work [20] used quantified features to make SFBCs distinguishable, nevertheless, it has low performance for low signal-to-noise ratio (SNR) and higher computational complexity.

In order to improve the performance and reduce the complexity, in this paper, we propose an extended SFBC identification algorithm for MIMO-OFDM transmissions over frequency-selective channels. First, we derive a discriminating feature vector for different SFBCs by analyzing the signal subspace and noise subspace of the received signals at adjacent OFDM sub-carriers. Then, the discriminating vector is calculated via a serial binary hypothesis test based on an asymptotically accurate expression from random matrix theory (RMT). Furthermore, we propose a decision tree based scheme which uses a special distance metric to provide a better identification performance with a short observation period in the low SNR range and reduce the computational complexity. The proposed algorithm does not require *a priori* knowledge of signal parameters such as the number of transmit antennas, channel coefficients, modulation mode and noise power. In addition, the proposed algorithm can identify single-antenna (SA) and spatial multiplexing (SM) signals.

The main contributions of this paper are summarized as follows:

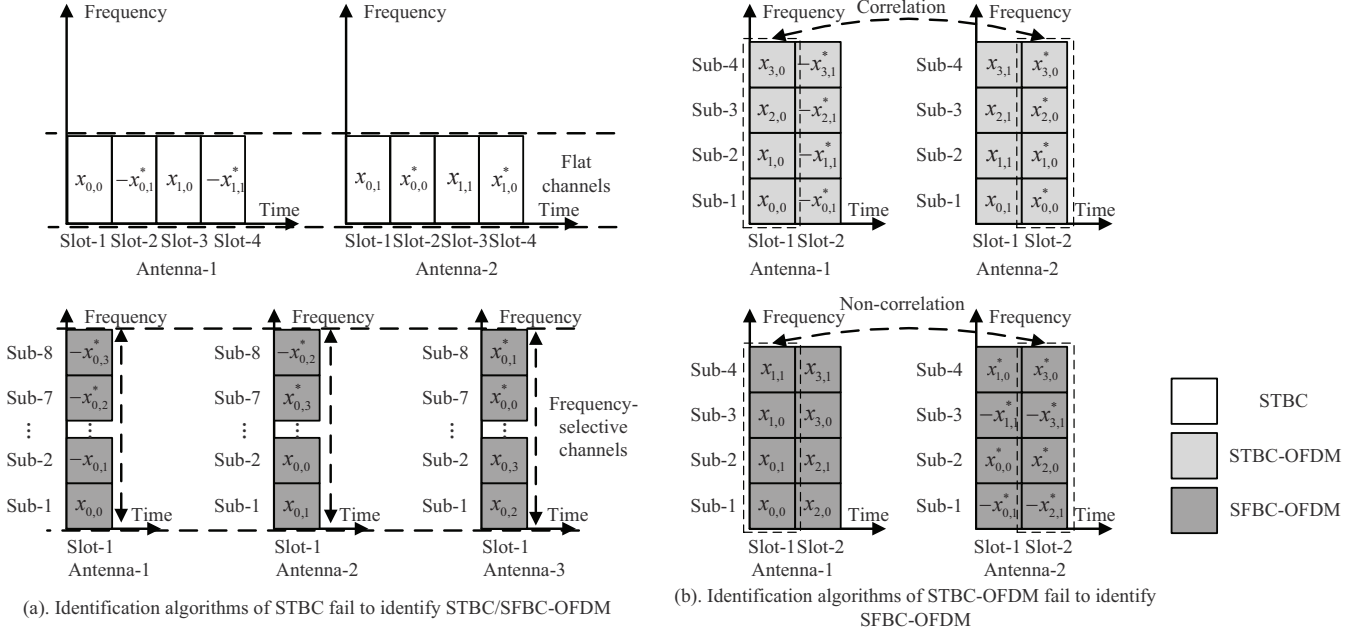


Fig. 1. Differences among the identification of STBC, STBC-OFDM and SFBC-OFDM.

- The proposed algorithm improves the performance of [20] by using an asymptotically accurate expression and a decision tree with a special distance metric.
- The proposed algorithm reduces the computational complexity of [20] by taking advantage of the tree's decision structure.
- The performance of the proposed algorithm is analyzed. An expression for a weak upper bound on the probability of correct identification is derived, and the consistency of the proposed algorithm is proved.
- Simulation results are presented to demonstrate the viability of the proposed algorithm with a short observation period in the low SNR range.

This paper is organized as follows. In Section II, the signal model is introduced. Section III describes the proposed algorithm, and in Section IV, the simulation setup and results are presented. Finally, conclusions are drawn in Section V.

Notation: Following notation is used throughout the paper. The superscripts $(\cdot)^*$, $(\cdot)^T$ and $(\cdot)^H$ denote complex conjugate, transposition and conjugate transposition, respectively. $\Pr\{B\}$ represents the probability of the event B . $\Pr\{B|A\}$ represents the conditional probability of the event B under the condition A . $E[\cdot]$ indicates statistical expectation. A complex value can be expressed as $\Re(\cdot) + j \cdot \Im(\cdot)$, where $\Re(\cdot)$ and $\Im(\cdot)$ denote the real and imaginary parts, respectively, and $j^2 = -1$. \mathbf{I} denotes the identity matrix. \mathbb{N} and \mathbb{Z}^+ denote the set of natural numbers and positive integer, respectively. The notation $d^{(v)}$ represents the symbol d at the v -th transmit or receive antenna.

II. PRELIMINARIES

A. Conventional Identification of STBC

The identification of STBC is the process of classifying the SM or STBC signals, which utilizes space-time redundancy to

reduce the error rate. From a practical point of view, STBC has three forms, including single-carrier STBC, STBC-OFDM and SFBC-OFDM. For single-carrier systems, the STBC encoder takes the row of an $N_t \times L$ STBC codeword matrix to span L consecutive time slots and maps every column of the matrix into N_t different transmit antennas, where the redundancy is between consecutive time slots. In STBC-OFDM, the STBC codeword is implemented at the same sub-carriers of consecutive OFDM symbols. Different from STBC-OFDM, the SFBC-OFDM encoder takes the row of the codeword matrix to span L consecutive sub-carriers directly, where the redundancy is between consecutive sub-carriers. Unfortunately, the existing algorithms of single-carrier STBC and STBC-OFDM can not be directly employed to identify SFBC-OFDM since the three forms of STBC have different received signal waveforms. Fig. 1 (a) shows that the identification algorithms of single-carrier STBC fail to identify STBC/SFBC-OFDM signals since the received signals are degraded by multipath effects. Fig. 1 (b) shows that the identification algorithms of STBC-OFDM can not identify SFBC-OFDM either since the signals between consecutive time slots are non-correlated in SFBC-OFDM.

B. System Model

We consider a MIMO-OFDM wireless communication system with N_t transmit antennas and M -PSK or M -QAM signal constellations ($M \geq 4$). Here, the transmitted symbols are assumed to be independent and identically distributed (i.i.d.), and the average modulated symbol energy is normalized to one. Subsequently, the modulated data symbol stream is parsed into data blocks of N_s symbols, denoted by $\mathbf{x}_b = [x_{b,0}, \dots, x_{b,N_s-1}]^T$. The SFBC encoder takes a $N_t \times L$ SFBC codeword matrix, denoted by $\mathbf{C}(\mathbf{x}_b)$, to span L consecutive subcarriers in an OFDM symbol. The SFBC

codeword matrices for SM ($N_s = N_t, L = 1$) and Alamouti (AL) ($N_t = 2, N_s = 2, L = 2$) are shown in (1) and (2), respectively, below

$$\mathbf{C}^{\text{SM}}(\mathbf{x}_b) = [x_{b,0}, \dots, x_{b,N_t-1}]^T \quad (1)$$

$$\mathbf{C}^{\text{AL}}(\mathbf{x}_b) = \begin{bmatrix} x_{b,0} & x_{b,1} \\ -x_{b,1}^* & x_{b,0}^* \end{bmatrix}. \quad (2)$$

For SA, the matrix can be seen as SM with $N_t = 1$. The matrices for SFBC⁽¹⁾ ($N_t = 3, N_s = 4, L = 8$) defined in [27], SFBC⁽²⁾ ($N_t = 2, N_s = 3, L = 4$), and SFBC⁽³⁾ ($N_t = 2, N_s = 3, L = 4$) defined in [28] are given in the Appendix. The v -th row of the codeword matrix is transmitted from the v -th antenna. The symbols on each antenna are input to the N consecutive sub-carriers of one OFDM block denoted by

$$\mathbf{S}(\mathbf{x}_b, \dots, \mathbf{x}_{b+\frac{N}{L}-1}) = \left[\mathbf{C}(\mathbf{x}_b), \dots, \mathbf{C}(\mathbf{x}_{b+\frac{N}{L}-1}) \right]. \quad (3)$$

Then, an OFDM modulator generates the time-domain block, i.e., OFDM symbol, via N -point inverse fast Fourier transform and adds the last ν samples as a cyclic prefix.

At the receiver side, we assume an advanced receiver composed of N_r ($N_r > N_t$) antennas and perfect synchronization. Later on in the paper, the effect of imperfect synchronization will be discussed. Here, the synchronization parameters, including the starting time of the OFDM symbol, number of sub-carriers and CP length, are assumed to be estimated successfully and fed to the OFDM demodulator. Several blind synchronization algorithms, even for the relatively low-SNR regime by using the cyclostationarity principles, were described in [29]–[31]. The received OFDM symbols are first stripped of the cyclic prefix and then converted into the frequency-domain via an N -point fast Fourier transform by the OFDM demodulator. We can construct an $N_t \times 1$ transmitted signal vector, transmitting one column of $\mathbf{S}(\mathbf{x}_b, \dots, \mathbf{x}_{b+N/L-1})$, denoted by $\mathbf{s}_k = [s_k^{(1)}, s_k^{(2)}, \dots, s_k^{(N_t)}]^T$, and a $N_r \times 1$ received signal vector $\mathbf{y}_k = [y_k^{(1)}, y_k^{(2)}, \dots, y_k^{(N_r)}]^T$ at the k -th OFDM sub-carrier ($1 \leq k \leq N$). The channel is assumed to be a frequency-selective fading channel and the k -th subchannel is characterized by an $N_r \times N_t$ full-rank matrix of fading coefficients denoted by

$$\mathbf{H}_k = \begin{bmatrix} h_k^{(1,1)} & \dots & h_k^{(N_t,1)} \\ \vdots & \ddots & \vdots \\ h_k^{(1,N_r)} & \dots & h_k^{(N_t,N_r)} \end{bmatrix} \quad (4)$$

where $h^{(v_1, v_2)}$ represents the channel coefficient between the v_1 -th transmit antenna and the v_2 -th receive antenna. Then, the n -th ($n \in \mathbb{N}$) received signal at the k -th OFDM sub-carrier is described by the following signal model

$$\mathbf{y}_k(n) = \mathbf{H}_k \mathbf{s}_k(n) + \mathbf{w}_k(n) \quad (5)$$

where the $N_r \times 1$ vector $\mathbf{w}_k(n)$ represents the complex additive white Gaussian noise (AWGN) at the k -th OFDM sub-carrier with zero mean and covariance matrix $\sigma_w^2 \mathbf{I}_{N_r}$.

III. PROPOSED BLIND SFBC IDENTIFICATION ALGORITHM

In this section, the signals at adjacent OFDM sub-carriers are analyzed firstly. Subsequently, the dimension of the signal subspace at adjacent OFDM sub-carriers is used as the discriminating feature for different SFBCs. Using a sliding window in the frequency domain, a discriminating vector is constructed to identify SFBCs. For the estimation of the dimension, we employ a serial binary hypothesis test with an asymptotically accurate expression based on RMT to detect the maximum eigenvalue in the noise subspace. Finally, a decision tree combined with a special distance metric between the estimated discriminating vector and the theoretical one is proposed to compute the result.

A. Discriminating Feature

Although OFDM signals propagate through frequency selective fading channels, we can reasonably assume that adjacent subchannels degenerate to a flat fading channel since the severity of the fading at adjacent subchannels is virtually identical. Then, we have

$$\mathbf{H}_{k+1} = \mathbf{H}_k + \Delta\mathbf{H} \approx \mathbf{H}_k \quad (6)$$

where $\Delta\mathbf{H}$ is a small difference. Let us define the n -th transmitted block at the k -th pair of adjacent OFDM sub-carrier, denoted by an $N_t \times 2$ matrix $\mathbf{S}_k(n) = [\mathbf{s}_k(n), \mathbf{s}_{k+1}(n)]$. The n -th received block at the k -th pair of adjacent OFDM sub-carrier is expressed as

$$\mathbf{Y}_k(n) = \mathbf{H}_k \mathbf{S}_k(n) + \mathbf{W}_k(n) \quad (7)$$

where the noise block is $\mathbf{W}_k(n) = [\mathbf{w}_k(n), \mathbf{w}_{k+1}(n)]$. Let us define a vector which only contains independent symbols, denoted by $\tilde{\mathbf{x}} = [x_1, \dots, x_m]^T$, i.e., all the elements in vector $\tilde{\mathbf{x}}$ are independent from each other. Then, $\mathbf{S}_k(n)$ can be alternatively expressed as follows

$$\mathbf{S}_k(n) = [\mathbf{A}_1(k) \tilde{\mathbf{x}}_k(n), \mathbf{A}_2(k) \tilde{\mathbf{x}}_k(n)] \quad (8)$$

where the matrix \mathbf{A} is a symbol generator matrix and the $2N_t$ vector $\tilde{\mathbf{x}}_k(n)$ is

$$\tilde{\mathbf{x}}_k(n) = [\Re(\tilde{\mathbf{x}}_k^T(n)), \Im(\tilde{\mathbf{x}}_k^T(n))]^T. \quad (9)$$

For example, an AL block is transmitted at the k -th sub-carrier and its neighbor. Hence, the vector of independent symbols at the k -th and $(k+1)$ -th OFDM sub-carrier pairs is $\tilde{\mathbf{x}}_k = [x_1, x_2]^T$ and the symbol matrices $\mathbf{A}_1(k)$ and $\mathbf{A}_2(k)$ are

$$\mathbf{A}_1(k) = \begin{bmatrix} 1 & 0 & j & 0 \\ 0 & -1 & 0 & j \end{bmatrix} \quad \mathbf{A}_2(k) = \begin{bmatrix} 0 & 1 & 0 & j \\ 1 & 0 & -j & 0 \end{bmatrix}. \quad (10)$$

Another example is two AL blocks transmitted at adjacent OFDM sub-carriers, i.e., the second column of the former block transmitting at k -th OFDM sub-carrier and the first column of the latter block transmitting at $(k+1)$ -th OFDM sub-carrier. In this case, the vector of independent symbols

at the k -th and $(k+1)$ -th OFDM sub-carrier pairs is $\bar{\mathbf{x}}_k = [x_1, x_2, x_3, x_4]^T$, respectively. The symbol matrices are

$$\mathbf{A}_1(k) = \begin{bmatrix} 0 & 1 & 0 & 0 & 0 & j & 0 & 0 \\ 1 & 0 & 0 & 0 & -j & 0 & 0 & 0 \end{bmatrix}$$

$$\mathbf{A}_2(k) = \begin{bmatrix} 0 & 0 & 1 & 0 & 0 & 0 & j & 0 \\ 0 & 0 & 0 & -1 & 0 & 0 & 0 & j \end{bmatrix}. \quad (11)$$

By stacking the real and imaginary parts of the signals in (7), we obtain

$$\begin{bmatrix} \Re(\mathbf{Y}_k(n)) \\ \Im(\mathbf{Y}_k(n)) \end{bmatrix} = \bar{\mathbf{H}}_k \begin{bmatrix} \Re(\mathbf{S}_k(n)) \\ \Im(\mathbf{S}_k(n)) \end{bmatrix} + \begin{bmatrix} \Re(\mathbf{W}_k(n)) \\ \Im(\mathbf{W}_k(n)) \end{bmatrix} \quad (12)$$

where the $2N_r \times 2N_t$ matrix $\bar{\mathbf{H}}_k$ is given by

$$\bar{\mathbf{H}}_k = \begin{bmatrix} \Re(\mathbf{H}_k) & -\Im(\mathbf{H}_k) \\ \Im(\mathbf{H}_k) & \Re(\mathbf{H}_k) \end{bmatrix}. \quad (13)$$

Then, denote the transmitted block in (12) as a column vector $\tilde{\mathbf{s}}_k(n)$ of size $4N_t$, which is defined as

$$\tilde{\mathbf{s}}_k(n) = \text{vec} \left\{ \begin{bmatrix} \Re(\mathbf{S}_k(n)) \\ \Im(\mathbf{S}_k(n)) \end{bmatrix} \right\}. \quad (14)$$

Denote the received block and noise block as column vectors $\tilde{\mathbf{y}}_k(n)$, $\tilde{\mathbf{w}}_k(n)$ of size $4N_r$, which are respectively defined as

$$\tilde{\mathbf{y}}_k(n) = \text{vec} \left\{ \begin{bmatrix} \Re(\mathbf{Y}_k(n)) \\ \Im(\mathbf{Y}_k(n)) \end{bmatrix} \right\} \quad (15a)$$

$$\tilde{\mathbf{w}}_k(n) = \text{vec} \left\{ \begin{bmatrix} \Re(\mathbf{W}_k(n)) \\ \Im(\mathbf{W}_k(n)) \end{bmatrix} \right\} \quad (15b)$$

where $\text{vec}\{\cdot\}$ represents vectorization. Under these notations, Equation (12) is finally expressed as

$$\tilde{\mathbf{y}}_k(n) = (\mathbf{I}_2 \otimes \bar{\mathbf{H}}_k) \tilde{\mathbf{s}}_k(n) + \tilde{\mathbf{w}}_k(n) \quad (16)$$

where \otimes denotes the Kronecker product. The covariance matrix Σ_k of $\tilde{\mathbf{y}}_k(n)$ is

$$\begin{aligned} \Sigma_k &= \mathbb{E} [\tilde{\mathbf{y}}_k(n) \tilde{\mathbf{y}}_k^T(n)] \\ &= (\mathbf{I}_2 \otimes \bar{\mathbf{H}}_k) \mathbb{E} [\tilde{\mathbf{s}}_k(n) \tilde{\mathbf{s}}_k^T(n)] (\mathbf{I}_2 \otimes \bar{\mathbf{H}}_k^T) \\ &\quad + \mathbb{E} [\tilde{\mathbf{w}}_k(n) \tilde{\mathbf{w}}_k^T(n)]. \end{aligned} \quad (17)$$

Next, assume that m_k is the number of independent symbols of $\tilde{\mathbf{x}}_k(n)$. Since the transmitted symbol energy is normalized, we obtain

$$\mathbb{E} [\tilde{\mathbf{x}}_k(n) \tilde{\mathbf{x}}_k^T(n)] = \frac{1}{2} \mathbf{I}_{2m_k}. \quad (18)$$

Additionally, the covariance of the noise is

$$\mathbb{E} [\tilde{\mathbf{w}}_k(n) \tilde{\mathbf{w}}_k^T(n)] = \frac{\sigma_w^2}{2} \mathbf{I}_{4N_r}. \quad (19)$$

As a result, from (17), (18) and (19), Σ_k is given as

$$\Sigma_k = \frac{1}{2} (\mathbf{I}_2 \otimes \bar{\mathbf{H}}_k) \mathbf{M}_k \mathbf{M}_k^T (\mathbf{I}_2 \otimes \bar{\mathbf{H}}_k^T) + \frac{\sigma_w^2}{2} \mathbf{I}_{4N_r} \quad (20)$$

where the matrix \mathbf{M}_k is

$$\mathbf{M}_k = \begin{bmatrix} \Re(\mathbf{A}_1(k)) \\ \Im(\mathbf{A}_1(k)) \\ \Re(\mathbf{A}_2(k)) \\ \Im(\mathbf{A}_2(k)) \end{bmatrix}. \quad (21)$$

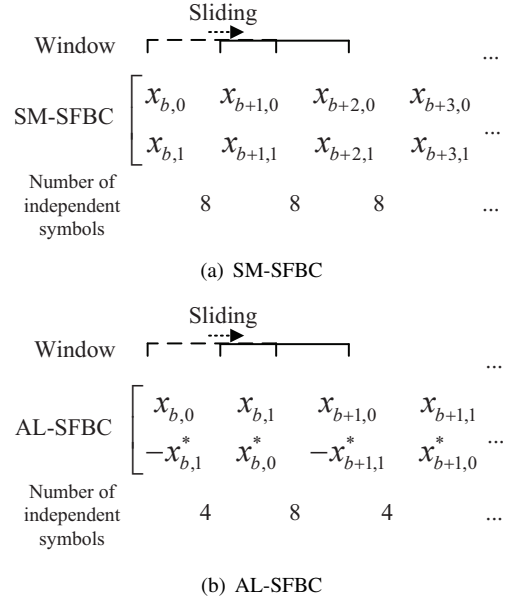


Fig. 2. Discriminating feature for SM-SFBC and AL-SFBC.

It is easy to verify that the rank of $(\mathbf{I}_2 \otimes \bar{\mathbf{H}})$ is full. We denote the eigenvalues of the covariance matrix Σ_k as $\lambda_1(k) \geq \dots \geq \lambda_{4N_r}(k)$.

Proposition: The smallest $4N_r - 2m_k$ ordered eigenvalues of Σ_k are all equal to $\sigma_w^2/2$, i.e.,

$$\lambda_{2m_k+1}(k) = \dots = \lambda_{4N_r}(k) = \sigma_w^2/2. \quad (22)$$

Proof: The rank of $\mathbf{M}_k \mathbf{M}_k^T$ can be easily shown to be $2m_k$, which makes the rank of the first term at the right hand side of (20) equal to $2m_k$. The smallest $4N_r - 2m_k$ ordered eigenvalues of $(\mathbf{I}_2 \otimes \bar{\mathbf{H}}_k) \mathbf{M}_k \mathbf{M}_k^T (\mathbf{I}_2 \otimes \bar{\mathbf{H}}_k^T)$ are equal to zero. Therefore, all of the smallest $4N_r - 2m_k$ ordered eigenvalues of Σ_k are equal to $\sigma_w^2/2$.

Actually, the number of independent symbols at the k -th OFDM sub-carrier and its neighbor, $2m_k$, is different for different SFBCs at different adjacent OFDM sub-carrier pairs. This number can be seen as the dimension of the signal subspace of the received signals at adjacent sub-carriers after separating the signal and noise subspace. By sliding a frequency-domain window, we can estimate the number of independent symbols for different adjacent OFDM sub-carrier pairs and then construct a discriminating feature vector as follows.

1) SM-SFBC: Without loss of generality, the case of 2 transmit antennas, SM⁽²⁾, is analyzed first, and the feature vectors of SA and SM⁽³⁾ are given afterwards. As shown in Fig. 2.a., the vectors of independent symbols for the first and second OFDM sub-carrier pairs are $\bar{\mathbf{x}}_1 = [x_{b,0}, x_{b,1}]^T$ and $\bar{\mathbf{x}}_2 = [x_{b+1,0}, x_{b+1,1}]^T$, respectively. Hence, the number at the first pair of adjacent OFDM sub-carriers, $2m_1$, is equal to 8. By moving the window, the vectors of independent symbols for the second and third OFDM sub-carrier pairs are $\bar{\mathbf{x}}_2 = [x_{b+1,0}, x_{b+1,1}]^T$ and $\bar{\mathbf{x}}_3 = [x_{b+2,0}, x_{b+2,1}]^T$, respectively. The number $2m_2$ is also equal to 8. Based on sliding the window, we construct a feature vector, denoted

by \mathbf{q} , whose elements are the numbers $2m_k$. For $\text{SM}^{(2)}$, the vector is $\mathbf{q}_{\text{SM}^{(2)}} = [8, 8, 8, 8, 8, 8, 8, 8, \dots]$. In addition, $\mathbf{q}_{\text{SA}} = [4, 4, 4, 4, 4, 4, 4, 4, \dots]$ is for SA, and $\mathbf{q}_{\text{SM}^{(3)}} = [12, 12, 12, 12, 12, 12, 12, 12, \dots]$ is for $\text{SM}^{(3)}$, respectively.

2) AL-SFBC: As shown in Fig. 2.b., the vectors of independent symbols for the first and second OFDM sub-carrier pairs are same as mentioned earlier, $\bar{\mathbf{x}}_1 = \bar{\mathbf{x}}_2 = [x_{b,0}, x_{b,1}]^T$. Hence, the number, $2m_1$, is equal to 4. After sliding the window to the next OFDM sub-carrier, the vectors of independent symbols for the second and third OFDM sub-carrier pairs are $\bar{\mathbf{x}}_2 = [x_{b,0}, x_{b,1}]^T$ and $\bar{\mathbf{x}}_3 = [x_{b+1,0}, x_{b+1,1}]^T$, respectively. The number $2m_2$ changes to 8. Consequently, the feature vector is $\mathbf{q}_{\text{AL}} = [4, 8, 4, 8, 4, 8, 4, 8, \dots]$.

3) Other SFBCs: Analogously, the feature vector of $\text{SFBC}^{(1)}$ is $\mathbf{q}_{\text{SFBC}^{(1)}} = [8, 8, 8, 8, 8, 8, 8, 12, \dots]$, that of $\text{SFBC}^{(2)}$ is $\mathbf{q}_{\text{SFBC}^{(2)}} = [6, 6, 6, 8, 6, 6, 6, 8, \dots]$, and $\mathbf{q}_{\text{SFBC}^{(3)}} = [6, 6, 6, 10, 6, 6, 6, 10, \dots]$ is for $\text{SFBC}^{(3)}$, respectively.

B. Classification of the Feature Vectors

First, we describe the method used to compute the k -th element of the estimated feature vector $\hat{\mathbf{q}}(k)$. According to (17), the estimated covariance matrix of the received vectorized signals is given by

$$\mathbf{R}_k = \frac{1}{N_b} \sum_{n=1}^{N_b} \tilde{\mathbf{y}}_k(n) \tilde{\mathbf{y}}_k(n)^T \quad (23)$$

where N_b is the number of OFDM symbols. The eigenvalues of \mathbf{R}_k are denoted by $l_1(k) \geq \dots \geq l_{4N_r}(k)$, which can be divided into the signal subspace $L_s = \{l_1(k), \dots, l_{2m_k}(k)\}$ and noise subspace $L_w = \{l_{2m_k+1}(k), \dots, l_{4N_r}(k)\}$. From Lemma 1 in [32], when $4N_r, N_b \rightarrow \infty, 4N_r/N_b \rightarrow \text{const} > 0$, the eigenvalue $l_{2m_k+1}(k)$ has asymptotically the same Tracy-Widom distribution as the largest eigenvalue of a pure noise Wishart matrix. The noise power $\sigma_w^2/2$ can be estimated by the average trace of L_w as $\frac{1}{4N_r - 2m_k} \sum_{i=2m_k+1}^{4N_r} l_i(k)$. Hence, the test statistic of the k -th pair of adjacent OFDM sub-carrier is constructed as

$$U_{2m_k+1}(k) = \frac{l_{2m_k+1}(k)}{\frac{1}{4N_r - 2m_k} \sum_{i=2m_k+1}^{4N_r} l_i(k)}. \quad (24)$$

Consequently, the distribution function of $U_{2m_k+1}(k)$ follows an asymptotically accurate expression as [33]

$$\Pr \left\{ \frac{U_{2m_k+1}(k) - \mu_{4N_r-2m_k, N_b}}{\xi_{4N_r-2m_k, N_b}} \leq z \right\} \approx F_{TW1}(z) - \frac{1}{(4N_r - 2m_k)N_b} \left(\frac{\mu_{4N_r-2m_k, N_b}}{\xi_{4N_r-2m_k, N_b}} \right)^2 F_{TW1}''(z) \quad (25)$$

where $F_{TW1}(\cdot)$ and $F_{TW1}''(\cdot)$ are the cumulative distribution functions of the Tracy-Widom distribution for the real value noise and its second-order derivative, respectively. The centering and scaling parameters, $\mu_{u,p}$ and $\xi_{u,p}$, respectively, are given as

$$\begin{cases} \mu_{u,p} = (\sqrt{u-0.5} + \sqrt{p-0.5})^2 \\ \xi_{u,p} = \sqrt{\mu_{u,p}} (1/\sqrt{u-0.5} + 1/\sqrt{p-0.5})^{1/3} \end{cases} \quad (26)$$

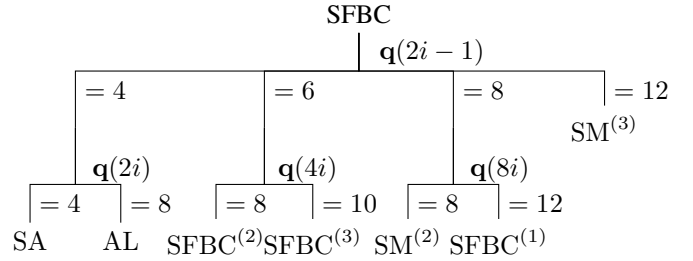


Fig. 3. Decision tree for the identification of SFBC.

where u and p are two parameters of the Wishart distribution. Specifically, u and p are the number of row and column of a random matrix, denoted by \mathbf{Y} , if the Wishart matrix is $\mathbf{W} = \mathbf{Y}\mathbf{Y}^T$. Then, the number $2m_k$ can be determined by a serial binary hypothesis test. Its decision criterion follows

$$\begin{cases} U_q(k) > \gamma_q, & \text{under } \mathcal{H}_1 \\ U_q(k) \leq \gamma_q, & \text{under } \mathcal{H}_0 \end{cases} \quad (27)$$

where $U_q(k)$ is the test statistic and γ_q is the threshold with $q = 1, 2, \dots, 4N_r$. The hypothesis \mathcal{H}_1 holds when the eigenvalue $l_q(k)$ corresponding to $U_q(k)$ is a signal eigenvalue ($l_q \in L_s$), while the hypothesis \mathcal{H}_0 holds when the eigenvalue $l_q(k)$ corresponding to $U_q(k)$ is a noise eigenvalue ($l_q \in L_w$). The threshold γ_q is

$$\gamma_q = F_{TW}^{-1}(1 - \text{Pr}_f) \xi_{4N_r-q+1, N_b} + \mu_{4N_r-q+1, N_b} \quad (28)$$

where $F_{TW}^{-1}(\cdot)$ is the inverse function of the right hand side (RHS) of Equation (25) and Pr_f is the false alarm probability. The steps of the test are that we let $q = 1, 2, \dots$ and compare $U_q(k)$ with γ_q until the first time that $U_q(k) \leq \gamma_q$. Then, the k -th element of $\hat{\mathbf{q}}$ is

$$\hat{\mathbf{q}}(k) = q - 1. \quad (29)$$

Subsequently, a decision tree classification is proposed to identify different SFBCs, as shown in Fig. 3. At the top-level node, we calculate $\hat{\mathbf{q}}(k)$ at odd-indexed adjacent sub-carrier pairs, where $k = 1, 3, \dots, 2i-1, \dots, N-1$ ($i \in \mathbb{Z}^+$), and compare the distance, denoted by d_c , between $\hat{\mathbf{q}}$ with odd-indexed elements and the theoretical values. The identified SFBC or subsets, denoted by \hat{C} , is the one which minimizes the distance d_c from the set of SFC = $\{\text{SFC}_1, \text{SFC}_2, \text{SFC}_3, \text{SM}^{(3)}\}$, given as

$$\hat{C} = \arg \min_{C \in \{\text{SFC}\}} d_c \quad (30)$$

where the top node yields 4-leaf branches. In this case, subsets $\text{SFC}_1, \text{SFC}_2, \text{SFC}_3$ and $\text{SM}^{(3)}$, are given by

$$\text{SFC}_1 = \{\text{SA}, \text{AL}\} \quad (31a)$$

$$\text{SFC}_2 = \{\text{SFBC}^{(2)}, \text{SFBC}^{(3)}\} \quad (31b)$$

$$\text{SFC}_3 = \{\text{SM}^{(3)}, \text{SFBC}^{(1)}\}. \quad (31c)$$

If the minimum distance is the same for two codes, the code with the smallest $\mathbf{q}(k)$ is selected. At second-level nodes, subsets $\text{SFC}_1, \text{SFC}_2$ and SFC_3 can be divided into corresponding SFBC codes according to $\hat{\mathbf{q}}(k)$ at different sub-carriers. Specifically, $k = 2, 4, \dots, 2i, \dots, N-2$ for the

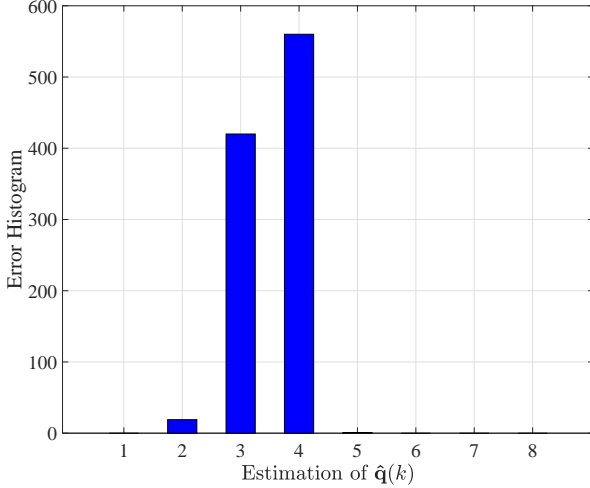


Fig. 4. Error histogram of the estimation of $\hat{q}(k)$, where correct number is 4 and $N_r = 8$, $N_b = 400$, $\text{SNR} = -1$ dB, $\text{Pr}_f = 10^{-4}$. The simulation was run for 1000 trials.

subset SFC_1 , $k = 4, 8, \dots, 4i, \dots, N-4$ for the subset SFC_2 and $k = 8, 16, \dots, 8i, \dots, N-8$ for the subset SFC_3 . Finally, Equation (30) is used to determine the result.

To improve the performance, we propose to compute a special distance metric d_c between $\hat{\mathbf{q}}$ and the theoretical one for possible sets and codes. The proposed distance d_c is

$$d_c = \left| \sum_k \varepsilon(\hat{\mathbf{q}}(k) - \mathbf{q}(k)) - \lceil N\text{Pr}_f \rceil \right| \quad (32)$$

where $|\cdot|$ represents the absolute value sign, $\varepsilon(\cdot)$ represents the unit step function, i.e., $\varepsilon(t) = \begin{cases} 1, t > 0 \\ 0, t \leq 0 \end{cases}$ and $\lceil \cdot \rceil$ indicates the ceiling function. The RHS of the distance formula is explained as follows:

- **The \sum terms:** The probability of underestimation when employing the serial hypothesis testing based on RMT is much larger than overestimation probability in the low SNR range, since signal eigenvalues are dominated by the noise. Fig. 4 shows that the correct $\hat{q}(k)$ is equal to 4 while the receiver determines a value of 3 far more than the value 5 at $\text{SNR} = -1$ dB. The performance gets worse if we employ the Euclidean distance [20] to compare the estimated vector $\hat{\mathbf{q}}$ with the theoretical one. Therefore, we use the unit step function. Once the estimated value is less than the theoretical one, the term should be set to zero.
- **The last term:** Overestimation still occurs due to the setting of Pr_f . However, ignoring overestimation will cause non-consensus estimation when processing more sub-carriers in the high SNR range. The conclusion of [33] proves that the expression (25) make Pr_f approximately accurate to describe the probability of overestimation of the test statistic U_{2m_k+1} for small and even moderate values of N_r and N_b ,

denoted by

$$\begin{aligned} \text{Pr}_o &\approx \text{Pr}_f \\ &\approx 1 - F_{TW1} \left(\frac{\gamma_q - \mu_{4N_r - 2m_k, N_b}}{\xi_{4N_r - 2m_k, N_b}} \right) \\ &\quad + \frac{1}{(4N_r - 2m_k) N_b} \left(\frac{\mu_{4N_r - 2m_k, N_b}}{\xi_{4N_r - 2m_k, N_b}} \right)^2 \\ &\quad F''_{TW1} \left(\frac{\gamma_q - \mu_{4N_r - 2m_k, N_b}}{\xi_{4N_r - 2m_k, N_b}} \right). \end{aligned} \quad (33)$$

Therefore, an error correction factor of $N\text{Pr}_f$, which represents the times of overestimation during N steps, should be subtracted in case of non-consensus estimations.

The proposed algorithm is summarized as follows

Summary of the proposed algorithm

Input: The observed symbols sequence \mathbf{y} .

Output: 7 types of SFBC code \hat{C} .

- 1: set $k = 1$
 - 2: **repeat**
 - 3: Vectorize the received block of adjacent sub-carriers and get $\tilde{\mathbf{y}}_k$ using (7), (12) and (15a)
 - 4: Compute the covariance matrix \mathbf{R}_k using (23)
 - 5: Eigenvalue decomposition of \mathbf{R}_k
 - 6: Construct the test statistic $U_q(k)$ using (24)
 - 7: Compute the threshold γ_q using (28)
 - 8: Estimate $\hat{\mathbf{q}}(k)$ using the serial hypothesis test by the decision criterion (27)
 - 9: $k = k + 2$
 - 10: **until** $k = N - 1$
 - 11: Get subsets in (31) **or** continue to the step 18 with $\hat{C} = \text{SM}^{(3)}$ using (32) and (30)
 - 12: According to the previous result, set $k = 2$ **or** 4 **or** 8
 - 13: **repeat**
 - 14: Step 3- Step 8
 - 15: $k = k + 2$ **or** $k + 4$ **or** $k + 8$
 - 16: **until** $k = N - 2$ **or** $N - 4$ **or** $N - 8$
 - 17: Obtain \hat{C} using (32) and (30)
 - 18: **return** \hat{C}
-

C. Performance and Consistency of our Algorithm

The accurate probability of correct identification is difficult to derive due to the heuristic \sum terms of the distance formula in (32). However, a weak upper bound of the probability on correct identification can be calculated by the probability of overestimation. The last term of (32) can tolerate $\lceil N\text{Pr}_f \rceil$ times of overestimation. Hence, an upper bound on the probability of correct identification of each level is

$$\text{Pr}_u = \sum_{i=0}^{\lceil N\text{Pr}_f \rceil} \binom{K}{i} \text{Pr}_o^i (1 - \text{Pr}_o)^{K-i} \quad (34)$$

where $\binom{K}{i} = \frac{K!}{i!(K-i)!}$ and K represents the number of estimations at each level. From *Theorem 5* in [32],

$$\lim_{N_b \rightarrow \infty} \text{Pr} \{ \hat{\mathbf{p}}(k) = 2m_k \} = 1 \quad (35)$$

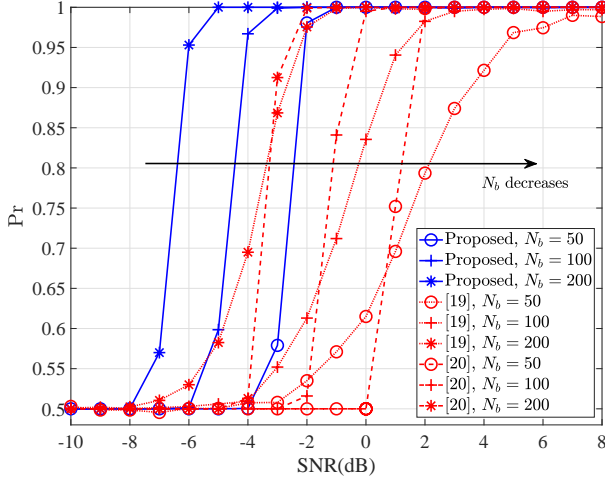


Fig. 5. Performance comparison of the proposed algorithm and the algorithms in [19], [20] for $N_t = 2$ and different N_b on the average probability of correct identification Pr , where the receiver has $N_r = 8$ antennas and the channel consists of $L_h = 6$ independent taps which follow a zero-mean complex Gaussian random variable with an exponential power delay profile, $\sigma_t^2 = e^{-t/5}$.

hence, $\lim_{N_b \rightarrow \infty} \text{Pr}_o = 0$. Then, we have

$$\lim_{\text{Pr}_o \rightarrow 0} \text{Pr}_u = \lim_{\text{Pr}_o \rightarrow 0} (1 - \text{Pr}_o)^K = 1. \quad (36)$$

IV. SIMULATION RESULTS

A. Simulation Setup

Monte Carlo simulation results are conducted to evaluate the performance of the proposed algorithm. Unless otherwise mentioned, we consider an SFBC-OFDM system with $N_r = 8$ receive antennas, $N = 128$ sub-carriers, cyclic prefix length $\nu = 10$, and 4-PSK modulation. The channel is assumed to be frequency-selective and consists of $L_h = 6$ statistically independent taps, each modeled as a zero-mean complex Gaussian random variable with an exponential power delay profile [19], $\sigma_t^2 = e^{-t/5}$. The probability of false alarm, Pr_f was set to 10^{-4} and the number of observed OFDM symbols N_b was 100. The average probability of correct identification Pr was used as a performance measure, defined as

$$\text{Pr} = \frac{1}{7} \sum \text{Pr}\{C|C\}. \quad (37)$$

The SFBC pool is set to $\{\text{SA}, \text{SM}^{(2)}, \text{AL}, \text{SFBC}^{(1)}, \text{SFBC}^{(2)}, \text{SFBC}^{(3)}, \text{SM}^{(3)}\}$. Simulation of each code was run for 1000 trials.

B. Performance Evaluation

1) *Case of two transmit antennas:* Actually, [19] only identified commonly used SFBCs, AL and $\text{SM}^{(2)}$. The number of receive antennas in [19] is also relatively small ($N_r = 2$ to 5). Indeed, that is an advantage for this algorithm. For a fair comparison in this paper, we assume that the number of transmit antennas is 2 and known by the receiver and the receiver has $N_r = 8$ antennas. This is a reasonable assumption because in some situations, for example, military applications,

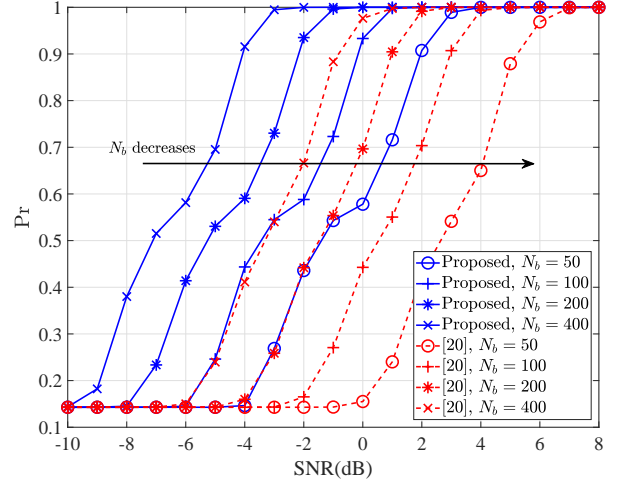


Fig. 6. Effect of the number of OFDM symbols, N_b , on the average probability of correct identification Pr .

additional antennas can be used to improve the performance. Fig. 5 shows the performance of the proposed algorithm in comparison with the algorithms in [19] and [20]. The set of time lags \mathcal{T} in [19] was set to $\{0, 1, 2, 3, 4, 5, 6\}$ with cardinality $|\mathcal{T}| = 7$ in case the performance is restricted. The results show that our proposed algorithm outperforms the algorithms in [19] and [20]. A 3-4 dB performance gain results from the proposed algorithm in comparison with [20], which reflects a more accurate estimation by utilizing the asymptotically accurate expression in (25) and the special distance formula in (32). Fig. 5 also shows that the proposed algorithm significantly outperforms the algorithm in [19] for a very short observation period.

2) *Unknown number of transmit antennas and effect of the number of OFDM symbols:* The algorithm in [19] cannot support a large SFBC pool. Next, a comparison between the proposed algorithm and the algorithm in [20] is provided. Fig. 6 shows the compared performance and the average probability of correct identification of the proposed algorithm for $N_b = 50$, $N_b = 100$, $N_b = 200$, $N_b = 400$. As expected, the proposed algorithm outperforms the algorithm in [20] significantly by about 2.5-3.5 dB. Additionally, the performance of the proposed algorithm improves with increasing N_b since a more accurate Tracy-Widom distribution is achieved. It is noteworthy that the performance of the proposed algorithm for $N_b = 100$ is between that of the algorithm in [20] for $N_b = 200$ and 400. This result indicates that the proposed algorithm performs well even for a short observation period.

3) *Evaluation of computational complexity:* Based on the number of floating point operations (flops) definitions in [34], the main computational complexities of the proposed algorithm and the algorithms in [19] and [20] are given by $48NN_r^3 + 24NN_bN_r^2$, $8N_b|\Xi|(N + \nu)(|\mathcal{T}| + 1)$ and $64NN_r^3 + 32NN_bN_r^2$, respectively. Here, the number of flops for the eigenvalue decomposition is $64N_r^3$ using the QR algorithm, and Ξ denotes the set of receive antenna pairs defined as $\Xi = \{(v_1, v_2) : v_1 \neq v_2, \text{ and } v_1 < v_2 \leq N_r\}$. In the previous

TABLE I
FLOPS COMPARISON BETWEEN THE PROPOSED ALGORITHM, THE ALGORITHMS IN [19], [20] FOR FOUR GROUPS OF PARAMETERS:
I. $N = 128, N_r = 4, N_b = 100$; II. $N = 64, N_r = 8, N_b = 100$; III. $N = 128, N_r = 8, N_b = 50$; IV. $N = 128, N_r = 8, N_b = 100$.

Identification algorithm	Main computational cost	Group I	Group II	Group III	Group IV
Proposed algorithm	$48NN_r^3 + 24NN_bN_r^2$	5,308,416	11,403,264	12,976,128	22,806,528
The algorithm in [19]	$8N_b \Xi (N + \nu)(\Upsilon + 1)$	5,299,200	13,260,800	12,364,800	24,729,600
The algorithm in [20]	$64NN_r^3 + 32NN_bN_r^2$	7,077,888	15,204,352	17,301,504	30,408,704

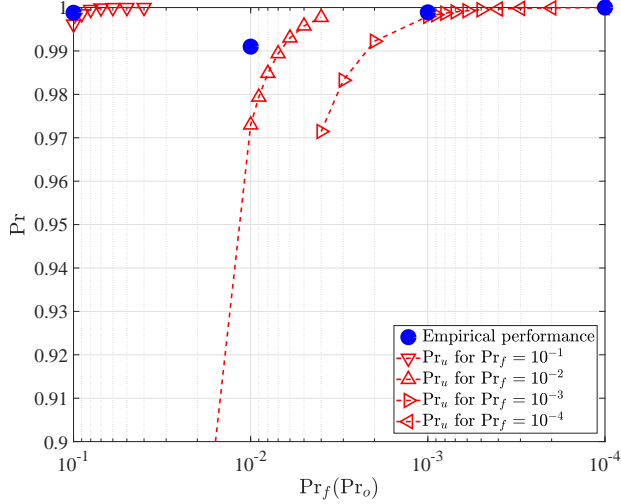


Fig. 7. Effect of the false alarm probability, \Pr_f , on the average probability of correct identification \Pr .

case, i.e., $N_r = 8, N = 128, \nu = 10, N_b = 100, |\Xi| = 28$ and $|\Upsilon| = 7$ and the proposed algorithm requires 22,806,528 flops. Employing the TMS320C6678 processor (a Digital Signal Processor produced by Texas Instruments) with 160 Giga-flops [35], the proposed algorithm requires only about 130 μs , while in the LTE standard, 7.14 ms are spent transmitting 100 OFDM symbols with one block duration of 71.4 μs [24]. The execution times of other algorithms are summarized in Table I. We can see that the proposed algorithm has comparable computational complexity to the algorithm in [19], although it achieves better performance as shown in Fig. 5. The proposed algorithm is also suitable for parallel implementation owing to the independence of eigenvalue decompositions at different sub-carriers. By employing field programmable gate arrays or CUDA-enabled graphics processing units, the computational complexity decreases N times.

C. Effect of the False Alarm Probability

In Fig. 7, we use the circle marker to show the simulation performance of the average probability of correct identification for different false alarm probabilities (horizontal axis represents \Pr_f). The SNR is set to 6 dB. Four dotted lines represent joint \Pr_u of the whole tree with the probability of overestimation \Pr_o for $\Pr_f = 10^{-1}, \Pr_f = 10^{-2}, \Pr_f = 10^{-3}$ and $\Pr_f = 10^{-4}$, respectively, using Equation (34) (horizontal axis changes to \Pr_o). We can see that the empirical points are very close to and a little higher than the theoretical points of the

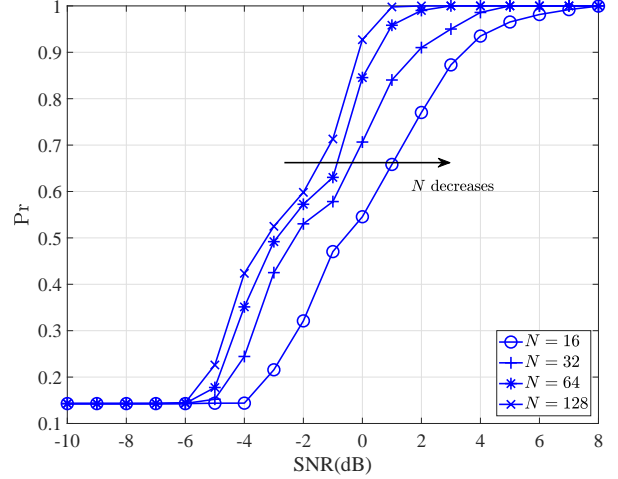


Fig. 8. Effect of the number of OFDM sub-carriers, N , on the average probability of correct identification \Pr .

upper bound since Equation (33) is an approximate formula which results in an error when substituting \Pr_f into \Pr_o . The results indicate that the performance decreases when the \Pr_f gets close to 0.01.

D. Effect of the Number of OFDM Subcarriers

Fig. 8 presents the average probability of correct identification of the proposed algorithm for different numbers of sub-carriers, N . The performance of the proposed algorithm improves when increasing N but with diminishing returns since the distance between the estimated $\hat{\mathbf{q}}$ and theoretical one converges rapidly with increasing N . In addition, a large N results in a large computational complexity.

E. Effect of the Number of Receive Antennas

Fig. 9 illustrates how the average probability of correct identification of the proposed algorithm is influenced by the number of receive antennas, N_r . With N_r increasing, the performance of the proposed algorithm improves because the estimation of the noise variance in the denominator of Equation (24) and the expression in (25) become more accurate.

F. Effect of the Modulation Type

Fig. 10 shows the average probability of correct identification of the proposed algorithm for different modulation types. The performance of the proposed algorithm does not depend on these modulation types, which are mandatory for

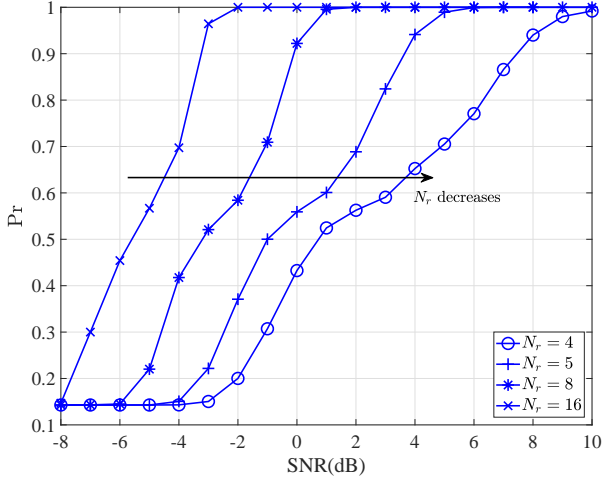


Fig. 9. Effect of the number of receive antennas, N_r , on the average probability of correct identification P_r .

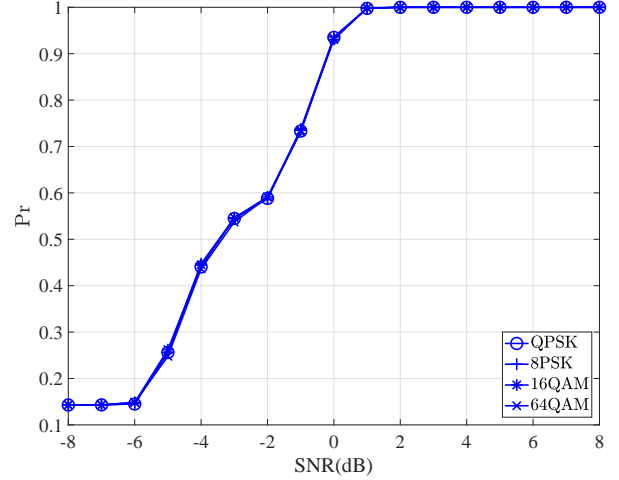


Fig. 10. Effect of the modulation type on the average probability of correct identification P_r .

most of the wireless standards. This is explained by the fact that the elements of the feature vector are determined by the matrix \mathbf{M}_k in (21) and is independent of the modulation type. However, the proposed algorithm fails when the transmitter emits real modulation signals because we stack the real and imaginary part of the signals, and the imaginary part will be zero for real modulation.

G. Effect of the Timing Offset

Perfect timing synchronization was assumed in this paper. Here, we evaluate the performance of the proposed algorithm in the presence of a timing offset. The sample timing offset (STO) is modeled as in [36], which depends on the location of the estimated FFT window starting point of OFDM symbols. The effects of STO are classified into the following four different cases:

- **Case I:** The window starting point coincides with the exact timing;
- **Case II:** The window starting point is before the exact timing, yet after the end of the channel response to the previous OFDM symbol;
- **Case III:** The window starting point is estimated to exist prior to the end of the channel response to the previous OFDM symbol. In this case, the orthogonality among sub-carriers is destroyed by the inter-symbol interference (ISI);
- **Case IV:** The window starting point is after the exact point, hence, the received signal includes the ISI and inter-channel interference (ICI).

Fig. 11 illustrates the performance of the proposed algorithm at SNR = 6 dB for different STOs and values of N . One can notice that the proposed algorithm mostly identifies correctly for a small forward offset, as in **Case II**, but fails for a large offset, as in **Case III** and **Case IV**, as the discriminating feature at an adjacent sub-carrier is destroyed by the ICI and ISI. However, the effect of the ISI will be dispersed under the condition of a large N with the improvement of performance [36].

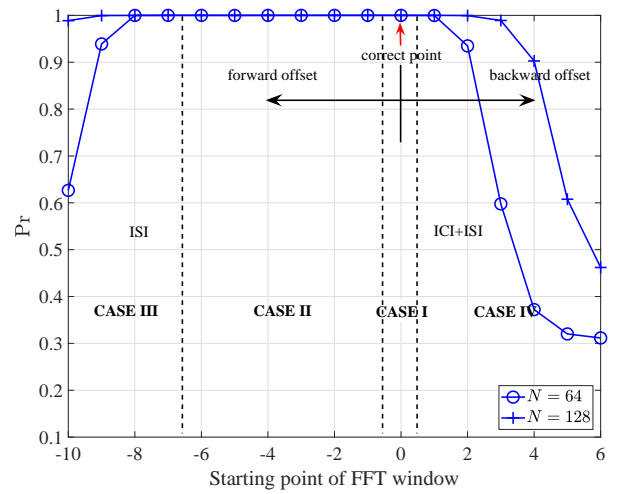


Fig. 11. Effect of the starting point of FFT window on the average probability of correct identification P_r at SNR = 6 dB.

H. Effect of the Frequency Offset

We consider the typical parameters of the LTE system to evaluate the impact of carrier frequency offset (CFO), with the number of sub-carriers being $N = 128$ (the channel bandwidths are 1.4 MHz), and the number of processed OFDM symbols is equal to $N_b = 50$ and $N_b = 100$. The algorithm in [20] are also compared with the proposed algorithm. The normalized carrier frequency offset is modeled as in [36]. Fig. 12 presents the effect of the normalized CFO to the sub-carrier spacing 15 kHz, Δf , on the performance at SNR = 4 dB and 6 dB. The results in Fig. 12 show that the proposed algorithm is robust for $\Delta f < 10^{-3}$ and outperforms the algorithm in [20] at a relatively low SNR for $N_b = 50$. Additionally, the proposed algorithm performs better for a reduced observation period since the ICI destroys the orthogonality of SFBCs [37] and this impact accumulates with increasing the number of the processed OFDM symbols. From a practical point of view, with the successful estimation of the starting points of OFDM

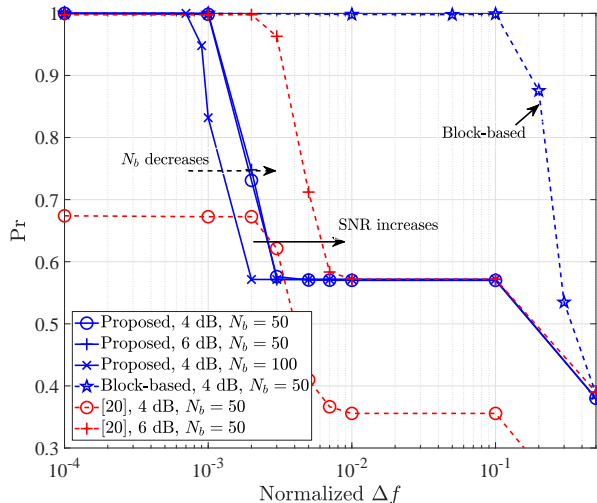


Fig. 12. Effect of the normalized CFO on the probability of correct identification Pr for the proposed algorithm and the algorithms in [19], [20] at SNR = 0 dB and 6 dB.

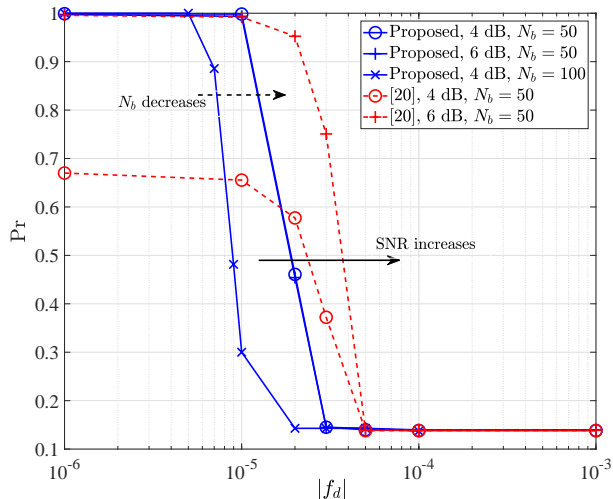


Fig. 13. Effect of the maximum Doppler spread on the probability of correct identification Pr for the proposed algorithm and the algorithms in [19], [20] at SNR = 0 dB and 6 dB.

symbols, we can use a block-based process that operates on each OFDM symbol by removing the CP and doing the FFT operation, and then aligning the starting point of the next OFDM symbol to ease the impact of CFO for a blind receiver. Fig. 12 shows the significant performance improvement using this block-based process. Furthermore, we can use a blind frequency offset compensation technique [38] by utilizing the kurtosis-type criterion before OFDM demodulation to reduce the effect of the frequency offset.

I. Effect of the Doppler

The previous analysis assumed static channels over the observation period. Typical parameters of the LTE standard with the channel bandwidth of 1.4 MHz ($N = 128$), sampling rate of 1.92 MHz and the number of processed OFDM symbols

being $N_b = 50$ and $N_b = 100$ are assumed here to evaluate the impact of the Doppler frequency on the performance of the proposed algorithm and the algorithm in [20]. Fig. 13 shows the probability of correct identification versus the maximum Doppler frequency normalized to the sampling rate, $|f_d|$, at SNR = 4 dB and 6 dB. The results show that the proposed algorithm outperforms the algorithm in [20] in the low-SNR regime with a small Doppler spread for a reduced observation period, and is robust for $|f_d| < 10^{-5}$ when $N_b = 50$.

V. CONCLUSIONS

We proposed a novel algorithm to identify SFBC-OFDM signals over frequency-selective channels. The dimension of the signal subspace of the received signals at adjacent subcarriers is proposed to be the discriminating feature after the analysis of the received signal subspace. Then, we construct a feature vector to classify different SFBCs, whose elements are estimated by using a serial binary hypothesis test based on an asymptotically accurate RMT expression. Furthermore, a decision tree and a special distance metric are proposed to reduce the computational complexity and improve the performance, respectively. The proposed algorithm does not need prior information about the number of transmit antennas, channel coefficients, modulation mode and noise power. The simulations demonstrated that the enhanced identification performance and reduced computational complexity are achieved under frequency selective fading with a short observation period. Future works include devising robust identification of SFBC schemes to address the effect of the frequency offsets and Doppler spreads.

APPENDIX

The orthogonal SFBC⁽¹⁾ of rate $\frac{1}{2}$ using $N_t = 3$ transmit antennas is defined by the following coding matrix [27]

$$\mathbf{C}^{\text{SFBC}^{(1)}}(\mathbf{x}_b) = \begin{bmatrix} x_{b,0} & x_{b,1} & x_{b,2} \\ -x_{b,1} & x_{b,0} & -x_{b,3} \\ -x_{b,2} & x_{b,3} & x_{b,0} \\ -x_{b,3} & -x_{b,2} & x_{b,1} \\ x_{b,0}^* & x_{b,1}^* & x_{b,2}^* \\ -x_{b,1}^* & x_{b,0}^* & -x_{b,3}^* \\ -x_{b,2}^* & x_{b,3}^* & x_{b,0}^* \\ -x_{b,3}^* & -x_{b,2}^* & x_{b,1}^* \end{bmatrix}^T. \quad (38)$$

The orthogonal SFBC⁽²⁾ of rate $\frac{3}{4}$ using $N_t = 3$ transmit antennas is defined by the following coding matrix [28]

$$\mathbf{C}^{\text{SFBC}^{(2)}}(\mathbf{x}_b) = \begin{bmatrix} x_{b,0} & 0 & x_{b,1} & -x_{b,2} \\ 0 & x_{b,0} & x_{b,2}^* & x_{b,1}^* \\ -x_{b,1}^* & -x_{b,2} & x_{b,0}^* & 0 \end{bmatrix}. \quad (39)$$

Last, the orthogonal SFBC⁽³⁾ of rate $\frac{3}{4}$ using $N_t = 3$ transmit antennas is defined by the following coding matrix [28]

$$\mathbf{C}^{\text{SFBC}^{(3)}}(\mathbf{x}_b) = \begin{bmatrix} x_{b,0} & -x_{b,1}^* & x_{b,2} & 0 \\ x_{b,1} & x_{b,0}^* & 0 & -x_{b,2}^* \\ x_{b,2} & 0 & -x_{b,0}^* & x_{b,1}^* \end{bmatrix}. \quad (40)$$

REFERENCES

- [1] Y. A. Eldemerdash, O. A. Dobre, and M. Öner, "Signal identification for multiple-antenna wireless systems: Achievements and challenges," *IEEE Commun. Surveys Tuts.*, vol. 18, no. 3, pp. 1524–1551, 3rd Quart 2016.
- [2] R. Liu and W. Trappe, *Securing Wireless Communications at the Physical Layer*, 1st ed. Springer Publishing Company, Incorporated, 2009.
- [3] O. Somekh, O. Simeone, Y. Bar-Ness, and W. Su, "Detecting the number of transmit antennas with unauthorized or cognitive receivers in MIMO systems," in *Proc. IEEE Mil. Commun. Conf. (MILCOM)*, Oct. 2007, pp. 1–5.
- [4] T. Li, Y. Li, L. Cimini, and H. Zhang, "Hypothesis testing based fast-converged blind estimation of transmit-antenna number for MIMO systems," *IEEE Trans. Veh. Technol.*, vol. PP, no. 99, pp. 1–1, 2018.
- [5] M. Mohammadkarimi, E. Karami, O. A. Dobre, and M. Z. Win, "Number of transmit antennas detection using time-diversity of the fading channel," *IEEE Trans. Signal Process.*, vol. 65, no. 15, pp. 4031–4046, Aug. 2017.
- [6] V. Choqueuse, M. Marazin, L. Collin, K. C. Yao, and G. Burel, "Blind recognition of linear space time block codes: A likelihood-based approach," *IEEE Trans. Signal Process.*, vol. 58, no. 3, pp. 1290–1299, Mar. 2010.
- [7] M. Shi, Y. Bar-Ness, and W. Su, "STC and BLAST MIMO modulation recognition," in *Proc. IEEE GLOBECOM*, Nov. 2007, pp. 3034–3039.
- [8] M. R. DeYoung, R. W. H. Jr., and B. L. Evans, "Using higher order cyclostationarity to identify space-time block codes," in *Proc. IEEE GLOBECOM*, Nov. 2008, pp. 1–5.
- [9] V. Choqueuse, K. Yao, L. Collin, and G. Burel, "Blind recognition of linear space time block codes," in *Proc IEEE Int. Conf. Acoust. Speech Signal Process. (ICASSP)*, Mar. 2008, pp. 2833–2836.
- [10] —, "Hierarchical space-time block code recognition using correlation matrices," *IEEE Trans. Wireless Commun.*, vol. 7, no. 9, pp. 3526–3534, Sept. 2008.
- [11] Y. A. Eldemerdash, M. Marey, O. A. Dobre, G. K. Karagiannidis, and R. Inkol, "Fourth-order statistics for blind classification of spatial multiplexing and Alamouti space-time block code signals," *IEEE Trans. Commun.*, vol. 61, no. 6, pp. 2420–2431, Jun. 2013.
- [12] M. Marey, O. A. Dobre, and R. Inkol, "Classification of space-time block codes based on second-order cyclostationarity with transmission impairments," *IEEE Trans. Wireless Commun.*, vol. 11, no. 7, pp. 2574–2584, Jul. 2012.
- [13] M. Mohammadkarimi and O. A. Dobre, "Blind identification of spatial multiplexing and Alamouti space-time block code via kolmogorov-smirnov (k-s) test," *IEEE Commun. Lett.*, vol. 18, no. 10, pp. 1711–1714, Oct. 2014.
- [14] M. Marey, O. A. Dobre, and B. Liao, "Classification of STBC systems over frequency-selective channels," *IEEE Trans. Veh. Technol.*, vol. 64, no. 5, pp. 2159–2164, May 2015.
- [15] M. Turan, M. Oner, and H. Cirpan, "Space time block code classification for MIMO signals exploiting cyclostationarity," in *Proc. IEEE Int. Conf. Commun. (ICC)*, Jun. 2015, pp. 4996–5001.
- [16] M. Marey, O. A. Dobre, and R. Inkol, "Blind STBC identification for multiple-antenna OFDM systems," *IEEE Trans. Commun.*, vol. 62, no. 5, pp. 1554–1567, May 2014.
- [17] Y. A. Eldemerdash, O. A. Dobre, and B. J. Liao, "Blind identification of SM and Alamouti STBC-OFDM signals," *IEEE Trans. Wireless Commun.*, vol. 14, no. 2, pp. 972–982, Feb. 2015.
- [18] E. Karami and O. A. Dobre, "Identification of SM-OFDM and AL-OFDM signals based on their second-order cyclostationarity," *IEEE Trans. Veh. Technol.*, vol. 64, no. 3, pp. 942–953, Mar. 2015.
- [19] M. Marey and O. A. Dobre, "Automatic identification of space-frequency block coding for OFDM systems," *IEEE Trans. Wireless Commun.*, vol. 16, no. 1, pp. 117–128, Jan. 2017.
- [20] M. Gao, Y. Li, T. Li, X. Lu, and H. Zhang, "Blind identification of MIMO-SFBC signals over frequency-selective channels," in *Proc. IEEE Wireless Commun. Netw. Conf. (WCNC)*, Mar. 2017, pp. 1–5.
- [21] M. Gao, Y. Li, L. Mao, H. Zhang, and N. Al-Dhahir, "Blind identification of SFBC-OFDM signals using two-dimensional space-frequency redundancy," in *Proc. IEEE GLOBECOM*, Dec. 2017, pp. 1–6.
- [22] "Information technology–telecommunications and information exchange between systems local and metropolitan area networks–specific requirements part 11: Wireless LAN medium access control (MAC) and physical layer (PHY) specifications," *ISO/IEC/IEEE 8802-11:2012(E) (Revision of ISO/IEC/IEEE 8802-11-2005 and Amendments)*, pp. 1–2798, Nov. 2012.
- [23] A. Stamoulis and N. Al-Dhahir, "Impact of space-time block codes on 802.11 network throughput," *IEEE Trans. Wireless Commun.*, vol. 2, no. 5, pp. 1029–1039, Sept. 2003.
- [24] S. Sesia, I. Toufik, and M. Baker, *LTE: The UMTS Long Term Evolution*. Wiley Online Library, 2009.
- [25] "IEEE standard for wirelessman-advanced air interface for broadband wireless access systems," *IEEE Std 802.16.1-2012*, pp. 1–1090, Sept. 2012.
- [26] R. Calderbank, S. Das, N. Al-Dhahir, and S. Diggavi, "Construction and analysis of a new quaternionic space-time code for 4 transmit antennas," *Communications in Information & Systems*, vol. 5, no. 1, pp. 97–122, Jan. 2005.
- [27] V. Tarokh, H. Jafarkhani, and A. R. Calderbank, "Space-time block codes from orthogonal designs," *IEEE Trans. Inf. Theory*, vol. 45, no. 5, pp. 1456–1467, Jul. 1999.
- [28] E. G. Larsson, P. Stoica, and G. Ganesan, *Space-Time Block Coding for Wireless Communications*. New York, NY, USA: Cambridge University Press, 2003.
- [29] A. Punctihewa, Q. Zhang, O. A. Dobre, C. Spooner, S. Rajan, and R. Inkol, "On the cyclostationarity of OFDM and single carrier linearly digitally modulated signals in time dispersive channels: Theoretical developments and application," *IEEE Trans. Wireless Commun.*, vol. 9, no. 8, pp. 2588–2599, Aug. 2010.
- [30] A. Punctihewa, V. K. Bhargava, and C. Despina, "Blind estimation of OFDM parameters in cognitive radio networks," *IEEE Trans. Wireless Commun.*, vol. 10, no. 3, pp. 733–738, Mar. 2011.
- [31] Z. Sun, R. Liu, and W. Wang, "Joint time-frequency domain cyclostationarity-based approach to blind estimation of OFDM transmission parameters," *EURASIP Journal on Wireless Communications and Networking*, vol. 2013, no. 1, pp. 117–125, Apr. 2013.
- [32] S. Kritchman and B. Nadler, "Non-parametric detection of the number of signals: Hypothesis testing and random matrix theory," *IEEE Trans. Signal Process.*, vol. 57, no. 10, pp. 3930–3941, Oct. 2009.
- [33] B. Nadler, "On the distribution of the ratio of the largest eigenvalue to the trace of a wishart matrix," *Journal of Multivariate Analysis*, vol. 102, no. 2, pp. 363–371, Oct. 2011.
- [34] D. S. Watkins, *Fundamentals of Matrix Computations*. Springer, 2002.
- [35] TI. TMS320C6678 fixed/floating point digital signal processor. [Online]. Available: <http://www.ti.com/product/tms320c6678>
- [36] Y. S. Cho, J. Kim, W. Y. Yang, and C. G. Kang, *MIMO-OFDM Wireless Communications with MATLAB*. Wiley Publishing, 2010.
- [37] S. Lu, B. Narasimhan, and N. Al-Dhahir, "A novel SFBC-OFDM scheme for doubly selective channels," *IEEE Trans. Veh. Technol.*, vol. 58, no. 5, pp. 2573–2578, Jun. 2009.
- [38] Y. Yao and G. B. Giannakis, "Blind carrier frequency offset estimation in SISO, MIMO, and multiuser OFDM systems," *IEEE Trans. Commun.*, vol. 53, no. 1, pp. 173–183, Jan. 2005.